



1 **Averaging over spatiotemporal heterogeneity substantially biases evapotranspiration rates in a mechanistic**
2 **large-scale land evaporation model**

3 Elham Rouholahnejad Freund^{1,2,3}, Massimiliano Zappa⁴, James W. Kirchner^{3,4,5}

4

5 ¹Laboratory of Hydrology and Water Management, Ghent University, Ghent, Belgium

6 ²Chair of Hydrology, Faculty of Environment and Natural Resources, University of Freiburg, Freiburg, Germany

7 ³Department of Environmental Systems Science, ETH Zurich, CH-8092 Zürich, Switzerland

8 ⁴Swiss Federal Research Institute WSL, CH-8903 Birmensdorf, Switzerland

9 ⁵Department of Earth and Planetary Science, University of California, Berkeley, CA 94720 USA

10

11 Correspondence to: Elham Rouholahnejad Freund, elham.rouholahnejad@gmail.com

12

13 **Abstract**

14 Evapotranspiration (ET) influences land-climate interactions, regulates the hydrological cycle, and contributes
15 to the Earth's energy balance. Due to its feedbacks to large-scale hydrological processes and its impact on
16 atmospheric dynamics, ET is a key driver of droughts and heatwaves. Existing land surface models differ
17 substantially, both in their estimates of current ET fluxes and in their projections of how ET will evolve in the
18 future. Any bias in estimated ET fluxes will affect the partitioning between sensible and latent heat, and thus
19 alter model predictions of temperature and precipitation. One potential source of bias is the so-called
20 "aggregation bias" that arises whenever nonlinear processes, such as those that regulate ET fluxes, are
21 modeled using averages of heterogeneous inputs. Here we demonstrate a general mathematical approach to
22 quantifying and correcting for this aggregation bias, using the GLEAM land evaporation model as a relatively
23 simple example. We demonstrate that this aggregation bias can lead to substantial overestimates in ET fluxes
24 in a typical large-scale land surface model when sub-grid heterogeneities in land surface properties are
25 averaged out. Using Switzerland as a test case, we examine the scale-dependence of this aggregation bias and
26 show that it can lead to overestimation of daily ET fluxes by as much as 21% averaged over the whole country.
27 We show how our approach can be used to identify the dominant drivers of aggregation bias, and to estimate
28 sub-grid closure relationships that can correct for aggregation biases in ET estimates, without explicitly
29 representing sub-grid heterogeneities in large-scale land surface models.

30 **Plain Language Summary**

31 Evapotranspiration (ET) is the largest flux from the land to the atmosphere and thus contributes to Earth's
32 energy and water balance. Due to its impact on atmospheric dynamics, ET is a key driver of droughts and
33 heatwaves. In this paper, we demonstrate how averaging over land surface heterogeneity contributes to
34 substantial overestimates of ET fluxes. We also demonstrate how one can correct for the effects of small-scale
35 heterogeneity without explicitly representing it in land surface models.



36

37 **1. Introduction**

38 Earth's surface and subsurface are characterized by spatial heterogeneity spanning wide ranges of scales,
39 including scales that cannot be explicitly resolved by large-scale Earth System Models (ESMs), which are
40 typically run at resolutions of 10-100 kilometers. Averaging over this finer-scale heterogeneity can bias model
41 estimates of water and energy fluxes and hence alter future temperature predictions. Earth system model
42 estimates of global terrestrial evaporation differ substantially from atmospheric reanalyses based on in-situ
43 and satellite remote sensing observations (Mueller et al., 2013), but it is unclear how much of these
44 differences could be attributed to errors in capturing sub-grid heterogeneity.

45

46 Several recent studies (e.g., Fan et al., 2019; Shrestha et al., 2018) have emphasized the need to account for
47 land surface heterogeneity in large-scale ESMs. Despite recent community efforts in refining ESMs' spatial
48 resolution (Huang et al., 2016; Rauscher et al., 2010; Ringler et al., 2008; Skamarock et al., 2012; Zarzycki et al.,
49 2014), the grid resolution of present-day ESMs is still too coarse to explicitly capture important effects of
50 surface heterogeneity. Whether the solution lies in hyper-resolution large-scale land surface modeling remains
51 an open question, because heterogeneities that are important to land-atmosphere fluxes will not be fully
52 resolved even at scales of 100 m (Beven and Cloke, 2012).

53

54 The effects of aggregating over spatial heterogeneity in land surface models have been assessed using several
55 approaches. Most of these approaches compare grid-cell-averaged energy and water fluxes with flux estimates
56 for finer-resolution grids, or for grid cells that are subdivided into mosaics of several surface types which
57 separately exchange momentum, energy, and water vapor with the overlying atmosphere (e.g., Giorgi, 1997).
58 Several studies have reported increases in average evapotranspiration (ET), and at least one has reported
59 decreases in grid-cell average ET, as model grids are coarsened and less spatial heterogeneity is accounted for
60 (e.g., Kuo et al., 1999; Boone and Wetzel, 1998; Hong et al., 2009; McCabe and Wood, 2006; Ershadi 2013; El
61 Maayar and Chen, 2006). Shrestha et al. (2018) studied the effects of horizontal grid resolution on ET
62 partitioning in the TerrSysMP Earth system model and found that the aggregation of topography decreases
63 average slope gradients and obscures small-scale convergence and divergence zones, directly impacting
64 surface and subsurface flow. They observed 5 and 8 percent decreases in the transpiration/evapotranspiration
65 ratio for a dry and a wet year, respectively, when their model grid cells were coarsened from 120 m to 960 m.
66 All these studies calculate the effects of land surface heterogeneity on ET fluxes using numerical experiments
67 that refine the model's spatial resolution, either directly or through the use of land-surface mosaics.

68

69 Quantifying the effect of sub-grid scale heterogeneity on grid-cell-averaged fluxes is especially important when
70 highly nonlinear processes are involved. Regardless of scale, the main challenge is not to explicitly represent
71 the heterogeneity in all its details, but instead to define an appropriate scale-dependent sub-grid closure
72 relationship that recognizes the important heterogeneities within the grid elements and the nonlinearities in



73 the processes (Beven, 2006). Such a sub-grid closure scheme would capture the effects of sub-grid
74 heterogeneity in large-scale land surface models without forcing them to run at finer spatial resolutions.
75
76 We have recently proposed a general theoretical framework, based on Taylor series expansions, that
77 quantifies the "aggregation bias" that results from averaging over sub-grid heterogeneity when grid-cell-
78 averaged ET is estimated (Rouholahnejad Freund and Kirchner, 2017; Rouholahnejad Freund et al., 2019). In
79 contrast to the numerical experiments described above, this theoretical framework does not depend on a
80 particular evapotranspiration model or grid scale. Our previous work demonstrated this framework using
81 Budyko curves as a see-through "toy" model, leaving open the question of how strongly ET estimates would be
82 affected by sub-grid heterogeneity in a more typical mechanistic evapotranspiration model. Here we use the
83 mechanistic evapotranspiration model GLEAM to quantify how aggregation biases vary across a range of
84 scales, using Switzerland as a case study. We show how our Taylor expansion framework can be used to
85 quantify the sensitivity of ET fluxes to heterogeneity in their individual drivers. We further demonstrate how
86 this framework can be used to estimate correction factors (i.e., sub-grid closure relationships) that account for
87 the effects of sub-grid heterogeneity without explicitly modeling it, and show how these correction factors can
88 be used to improve grid-scale ET estimates. Because our framework is not model-specific, the analysis
89 presented here could also be applied to many other evapotranspiration algorithms.

90

91 **2. Methods and results**

92 **2.1. A common mechanistic framework for predicting evapotranspiration**

93 Most large-scale land surface models calculate ET as a function of available water and energy at daily time
94 steps. They typically multiply an estimate of potential evapotranspiration (PET) by a conversion factor to
95 calculate actual evapotranspiration. PET is generally understood as the maximum rate of evapotranspiration
96 from a large area (to avoid the effect of local advection) covered completely and uniformly by actively growing
97 vegetation with adequate moisture at all times (Brutseart, 1984). Models typically estimate PET using the
98 Penman equation (Penman, 1948; intended for open water surfaces), the Penman-Monteith equation
99 (Monteith, 1965, Monteith and Unsworth, 1990; intended for reference crop evapotranspiration by adding
100 atmospheric transport processes and stomatal resistance to Penman's open water evaporation), or the
101 Priestley-Taylor equation (Priestley and Taylor, 1972; intended for open water and water-saturated crops and
102 grasslands). The conversion factor that is used to estimate ET from PET typically depends on plant physiology
103 and on the water that is available for evaporation.

104

105 Here, we employ an ET algorithm that is used by several land surface models (i.e., Global Land-surface
106 Evaporation: The Amsterdam Methodology (GLEAM); Miralles et al., 2011; Martens et al., 2017), in which
107 actual ET is calculated as a fraction of PET. This fraction is expressed as a multiplicative factor, often called a
108 stress factor, which ranges between 0 and 1 and thus limits ET rates. Under wet conditions, ET can equal PET
109 (stress factor equals one) while under dry conditions, PET is multiplied by a stress factor smaller than one
110 depending on the degree of water stress. This approach is employed by the GLEAM model, among others.



111 GLEAM is a diagnostic satellite-data-driven method that is used to estimate global land evaporation fluxes.
112 GLEAM uses the Priestley-Taylor formula and remotely sensed datasets of radiation and temperature to
113 calculate PET. In GLEAM, actual ET is calculated by constraining PET estimates by a stress factor that is based
114 on estimates of root-zone soil moisture. The root zone soil moisture is derived from a multi-layer water
115 balance module that describes the infiltration of precipitation through the vertical soil profile. ET estimates
116 from GLEAM have been applied in many studies (e.g., Miralles et al., 2013; Miralles et al., 2014; Greve et al.,
117 2014; Jasechko et al., 2013). GLEAM operates on daily time steps at 0.25-degree spatial resolution. To the best
118 of our knowledge, there are no prior studies quantifying the aggregation bias in ET estimates from GLEAM or
119 other models with similar ET formulations.

120

121 GLEAM calculates ET as an explicit function of the stress factor and potential evaporation:

$$122 \quad ET = S \cdot PET + (1 - \beta) I, \quad (1)$$

123 where ET is actual evapotranspiration (mm d^{-1}), S is the evaporative stress factor (-) that accounts for
124 environmental conditions that reduce actual ET relative to potential ET, I is interception losses (mm d^{-1}), and β
125 is a constant ($\beta = 0.07$ – Gash and Stewart, 1977) that avoids double-counting of interception losses during
126 hours with wet canopy. The stress factor (S) depends on the soil moisture conditions, and is parametrized
127 separately for tall canopy, short vegetation, and bare soil. GLEAM uses the following soil-moisture-based
128 parameterization to calculate the stress factor (Miralles et al., 2011; Martens et al., 2017):

$$129 \quad S = 1 - \left(\frac{w_c - w_w}{w_c - w_{wp}} \right)^2, \quad (2)$$

130 where S is the stress factor (-) for tall canopy, w_w is the volumetric soil moisture at any given time ($\text{m}^3 \text{m}^{-3}$), and
131 w_c and w_{wp} are the critical soil moisture level and soil moisture at wilting point. For soil moisture values below
132 the wilting point w_{wp} , the stress is maximal (stress factor equals 0), causing ET to sharply decline to zero. For
133 values above the critical moisture level w_c , there is no water stress (stress factor equals 1) and ET equals PET.
134 Between w_{wp} and w_c the stress increases as soil moisture decreases following a parabolic function (Eq. 2). In
135 the analysis presented below, we set the critical soil moisture level (w_c) and soil moisture at wilting point
136 (w_{wp}) to 0.6 and 0.1 $\text{m}^3 \text{m}^{-3}$ respectively. To simplify the analysis presented below, we have used the tall-
137 canopy stress factor (Eq. 2) for all of Switzerland, even though the short-canopy or bare-soil formulations may
138 be better suited to some locations.

139

140 GLEAM uses the Priestley-Taylor approach to calculate PET (Priestley and Taylor, 1972):

$$141 \quad PET = \frac{\alpha}{\lambda} \frac{\Delta}{\Delta + \gamma} (R_n - G), \quad (3)$$

142 where PET is potential evapotranspiration (mm d^{-1}), α is a dimensionless coefficient that parametrizes the
143 resistance to evaporation and is set to 0.8 for tall canopy in GLEAM (Miralles et al., 2011), $\lambda = 2.26$ (MJ kg^{-1}) is
144 the latent heat of vaporization, R_n is net radiation ($\text{MJ m}^{-2} \text{d}^{-1}$), G is the ground heat flux, approximated as
145 $G = 0.05 R_n$ ($\text{MJ m}^{-2} \text{d}^{-1}$) for tall canopy in GLEAM, T is temperature ($^{\circ}\text{C}$), and Δ is the slope of the



146 temperature/saturated vapor pressure curve ($\text{kPa}^\circ\text{C}^{-1}$), which is functionally related to temperature (Tetens,
 147 1930; Murray, 1967; Stanghellini, 1987):

$$148 \quad \Delta = ae^{bT}, \quad (4)$$

149 where $a=0.04145$ ($\text{kPa}^\circ\text{C}^{-1}$), $b=0.06088$ ($^\circ\text{C}^{-1}$), and γ is the psychrometric constant ($\text{kPa}^\circ\text{C}^{-1}$) which can be
 150 calculated as (Brunt, 1952):

$$151 \quad \gamma = \frac{C_{p\text{air}} * P}{\lambda * MW_{\text{ratio}}}, \quad (5)$$

152 where $C_{p\text{air}} = 0.001013$ ($\text{MJ kg}^{-1}^\circ\text{C}^{-1}$) is the specific heat of air at constant pressure, $P = 101.3$ (kPa) is
 153 atmospheric pressure, and $MW_{\text{ratio}} = 0.622$ (-) is the molecular weight ratio of $\text{H}_2\text{O}/\text{air}$. Substituting the
 154 aforementioned constants in Eq. 5 yields $\gamma = 0.073$ ($\text{kPa}^\circ\text{C}^{-1}$). Expanding Eq. 1 using Eqs. 2-5 yields the ET
 155 function as calculated by GLEAM:

$$156 \quad \begin{aligned} ET_{[\text{mmd}^{-1}]} &= \left[-4w_w[m^3m^{-3}]^2 + 4.8w_w[m^3m^{-3}] - 0.44 \right] * \frac{\alpha_{[\]}}{\lambda_{[\text{MJ kg}^{-1}]}} * \frac{\Delta_{[\text{kPa}^\circ\text{C}^{-1}]}}{\Delta_{[\text{kPa}^\circ\text{C}^{-1}]} + \gamma_{[\text{kPa}^\circ\text{C}^{-1}]}} \\ &* 0.95 * \frac{86400}{1000000} * R_n[w_m^{-2}] + (1 - \beta) I_{[\text{mmd}^{-1}]} \\ &= \left[-4w_w^2 + 4.8w_w - 0.44 \right] * 0.02905 * \frac{a e^{bT}}{a e^{bT} + 0.073} R_n + (1 - 0.07) I_{[\text{mmd}^{-1}]} \end{aligned} \quad (6)$$

157
 158 In the analysis below, we use GLEAM to demonstrate how aggregation biases can be estimated in land surface
 159 modeling schemes. We chose GLEAM because its governing equations are amenable to the analytical solutions
 160 derived below. Here we make no particular claim for the accuracy or validity of GLEAM as an
 161 evapotranspiration model, nor is our analysis intended to test this. Likewise our analysis should not be
 162 interpreted as implying that GLEAM is any more, or less, susceptible to aggregation bias than other
 163 evapotranspiration schemes, because this question is beyond the scope of the current paper.

164

165 2.2. Mathematical framework for predicting aggregation bias

166 *Nonlinear averaging using second-order Taylor expansions*

167 ET is a nonlinear function of its drivers. An intrinsic property of any nonlinear function is that the average of
 168 the function will not equal the function evaluated at the average inputs (e.g., Rastetter et al., 1992; Giorgi and
 169 Avissar, 1997). Thus averaging over sub-grid heterogeneity in ET drivers, as large-scale land surface models do,
 170 would be expected to lead to biased ET estimates, even if the underlying equations were exactly correct. For
 171 an ET function of three variables, namely R_n , w_w , and T , the mean of the ET function, in terms of the function's
 172 value at the mean of its inputs, can be approximated by the second-order Taylor series expansion of the ET
 173 function (Eq. 6):

$$174 \quad \begin{aligned} \overline{ET} \approx \widehat{ET} &+ \frac{1}{2} \left[\frac{\partial^2 ET}{\partial R_n^2} \text{Var}(R_n) + \frac{\partial^2 ET}{\partial w_w^2} \text{Var}(w_w) + \frac{\partial^2 ET}{\partial T^2} \text{Var}(T) \right] \\ &+ \frac{\partial^2 ET}{\partial R_n \partial T} \text{Cov}(R_n, T) + \frac{\partial^2 ET}{\partial R_n \partial w_w} \text{Cov}(R_n, w_w) + \frac{\partial^2 ET}{\partial w_w \partial T} \text{Cov}(w_w, T), \end{aligned} \quad (7)$$

175 where \overline{ET} is the estimate of the true average of the nonlinear ET function over its variable inputs, \widehat{ET} is the ET
 176 function evaluated at its mean inputs, and the derivatives are understood to be evaluated at the mean values



177 of the variables ($\bar{R}_n, \bar{w}_w, \bar{T}$). For the specific case of the GLEAM model, these derivatives are derived
 178 analytically from the ET function described by Eq. 6, directly yielding the following expressions:

$$179 \quad \widehat{ET} = [-4\bar{w}_w^2 + 4.8\bar{w}_w - 0.44] * 0.02905 * \frac{a e^{b\bar{T}}}{a e^{b\bar{T}} + 0.073} \bar{R}_n, \quad (8)$$

$$180 \quad \frac{\partial^2 ET}{\partial R_n^2} = 0, \quad (9)$$

$$181 \quad \frac{\partial^2 ET}{\partial w_w^2} = [-8] * 0.02905 * \frac{\Delta}{\Delta + \gamma} R_n \quad (w_{wp} \leq w_w \leq w_c), \quad (10a)$$

$$182 \quad \frac{\partial^2 ET}{\partial w_w^2} = 0 \quad (w_w < w_{wp}, \quad w_w > w_c), \quad (10b)$$

$$183 \quad \frac{\partial^2 ET}{\partial T^2} = [-4w_w^2 + 4.8w_w - 0.44] * 0.02905 * R_n * b^2 * \frac{\gamma^2 \Delta - \gamma \Delta^2}{(\gamma + \Delta)^3}, \quad (11)$$

$$184 \quad \frac{\partial^2 ET}{\partial R_n \partial T} = [-4w_w^2 + 4.8w_w - 0.44] * 0.02905 * \frac{\Delta}{\Delta + \gamma} * \frac{b\gamma}{\Delta + \gamma}, \quad (12)$$

$$185 \quad \frac{\partial^2 ET}{\partial R_n \partial w_w} = [-8w_w + 4.8] * 0.02905 * \frac{\Delta}{\Delta + \gamma} \quad (w_{wp} \leq w_w \leq w_c), \quad (13a)$$

$$186 \quad \frac{\partial^2 ET}{\partial R_n \partial w_w} = 0 \quad (w_w < w_{wp}, \quad w_w > w_c), \quad (13b)$$

$$187 \quad \frac{\partial^2 ET}{\partial w_w \partial T} = [-8w_w + 4.8] * 0.02905 * \frac{\Delta}{\Delta + \gamma} * \frac{b\gamma}{\Delta + \gamma} * R_n \quad (w_{wp} \leq w_w \leq w_c), \quad \text{and} \quad (14a)$$

$$188 \quad \frac{\partial^2 ET}{\partial w_w \partial T} = 0 \quad (w_w < w_{wp}, \quad w_w > w_c), \quad (14b)$$

189 where Δ depends on temperature as described in Eq. (4). The difference between the average of the functions
 190 (\widehat{ET}) and the function of the averages (\widehat{ET}), or, equivalently, the sum of all the other terms in Eq. (7),
 191 represents the aggregation bias. The magnitude of this bias can be calculated by combining Eqs. 7-14 with
 192 estimates of the variances and covariances of the input variables.

193

194 The approach outlined in Eq. (7) is general and could be extended to other land surface modeling schemes.
 195 The partial derivatives in Eqs. (8-14), of course, are specific to the GLEAM equations; for other models they
 196 would differ. More complex land surface model algorithms may not have such simple analytical derivatives; in
 197 that case, the derivatives can be evaluated numerically.

198

199 2.3. Sub-grid heterogeneity and aggregation bias in ET estimates across Switzerland

200 Drivers of ET (i.e., soil moisture, net radiation, and temperature) can be highly heterogeneous within the grid
 201 cells of typical ESMs. Soil moisture can show pronounced spatial variability, especially in areas where surface
 202 roughness, porosity, and permeability vary by orders of magnitude across a variety of length scales (Giorgi and
 203 Avissar, 1997). Temperature and incoming radiation vary significantly with season, elevation, altitude, and
 204 albedo. Switzerland, for example, shows strong local variations in average annual temperature, soil moisture
 205 content, net radiation, and albedo (Fig. 1; albedo values in Fig. S1).

206



207 We quantified how averaging over spatial (and temporal) heterogeneities of ET drivers affects estimated ET at
208 several grid scales across Switzerland, as an example case for which high-resolution data are available. Our
209 analysis is based on 500-m input data of temperature (interpolation of MeteoSwiss data after Viviroli et al.,
210 2009), net radiation (Viviroli et al., 2009), and soil moisture (simulations from the hydrological model PREVAH,
211 Brunner et al., 2019; Speich et al., 2015; Orth et al., 2015; Zappa et al., 2003) at daily time steps for the 2004
212 growing season. Although our soil moisture data are derived from model simulations whose accuracy is
213 difficult to assess due to the scarcity of real-world soil moisture measurements, for our purposes all that is
214 necessary is that the simulated values exhibit realistically complex spatial variability.

215

216 We used the GLEAM equations, as outlined in Sect. 2, to calculate ET for each day at the 500-m resolution of
217 these input data. We use these 500-m ET estimates as virtual "truth" for the purpose of our analysis, because
218 our goal is not to determine whether GLEAM estimates of ET are accurate (compared to direct measurements,
219 for example), but rather to quantify how spatial aggregation affects them.

220

221 To quantify how spatial aggregation affects model estimates of ET, we calculated ET over larger spatial scales
222 in two different ways. First, we averaged the 500-m ET estimates over 1/32, 1/16, 1/8, 0.25, 0.5, 0.75, 1, and 2-
223 degree grid cells across Switzerland, to represent the "true" average ET at those grid scales. Second, we
224 averaged the 500-m input data (of temperature, soil moisture, and net radiation) over the same grid cells, and
225 then used these grid-cell-averaged input data in the GLEAM equations to calculate the modeled coarse-
226 resolution ET at each grid scale. The deviation of the modeled coarse-resolution ET from the "true" average ET
227 measures the aggregation bias. Because this numerical experiment uses the same model equations, based on
228 the same underlying data, for the ET calculations at each spatial resolution, it isolates spatial aggregation as
229 the only possible cause of the difference between the "true" average ET (\overline{ET} in Eq. 7) and the coarse-resolution
230 modeled ET (\widehat{ET} in Eq. 7) at each grid scale.

231

232 Figure 2a shows that the ET aggregation bias varies considerably across Switzerland, and also varies
233 considerably with grid scale. The average aggregation bias is higher at coarser grid scales, averaging 21.4% at
234 2-degree grid resolution and 16.8% at 1-degree grid resolution across all of Switzerland (calculated as the
235 median of the daily aggregation biases over the growing season; Fig. 2a). Smaller grid scales typically exhibit
236 smaller aggregation biases (averaging 7% at 1/16-degree grid resolution across all of Switzerland calculated as
237 the median of the daily aggregation biases over the growing season) because they typically average over less
238 spatial heterogeneity, but even at the smallest grid scales, aggregation biases can locally exceed 68%, as
239 indicated by the red grid cells in Fig. 2a. These figures are medians for the entire growing season of 2004; the
240 aggregation biases of two randomly selected days (May 31st and July 21st, 2004) at several spatial scales are
241 much larger overestimation of ET in parts of southern Switzerland (Figs. S2, S3).

242

243 Using our 500-m input data, we can test how well Eq. (7) estimates the difference between the "true" average
244 ET and the coarse-resolution modeled ET at each grid scale. We used Eqs. (8-14) to calculate the partial



245 derivatives of the GLEAM equations for each grid cell and time step, using the grid-cell averaged values of the
246 input data. We then multiplied these derivatives by the corresponding variances and covariances among the
247 500-m input data to obtain bias estimates via Eq. (15) for each grid cell and time step:

$$\text{Bias} = \widehat{\text{ET}} - \overline{\text{ET}} \approx -\frac{1}{2} \left[\frac{\partial^2 \text{ET}}{\partial R_n^2} \text{Var}(R_n) + \frac{\partial^2 \text{ET}}{\partial w_w^2} \text{Var}(w_w) + \frac{\partial^2 \text{ET}}{\partial T^2} \text{Var}(T) \right] \\ - \frac{\partial^2 \text{ET}}{\partial R_n \partial T} \text{Cov}(R_n, T) - \frac{\partial^2 \text{ET}}{\partial R_n \partial w_w} \text{Cov}(R_n, w_w) - \frac{\partial^2 \text{ET}}{\partial w_w \partial T} \text{Cov}(w_w, T), \quad (15)$$

249 where $\overline{\text{ET}}$ is the true average ET at some grid resolution, $\widehat{\text{ET}}$ is the modeled coarse-resolution ET at the same
250 spatial scale, the right-hand side is the Taylor expansion estimate of the aggregation bias. We then compared
251 these estimated biases against the "true" aggregation biases (the difference between the "true" average ET
252 and the coarse-resolution modeled ET) in the numerical experiment described above. The true bias, in other
253 words, is $\widehat{\text{ET}} - \overline{\text{ET}}$ in Eq. (15), and the estimated bias is the Taylor approximation on the right-hand side.

254

255 Figure 2b shows that the aggregation bias estimated by Eq. (15) is generally similar, in both overall magnitude
256 and spatial distribution, to the "true" aggregation biases calculated by the numerical experiment. This
257 comparison is shown more explicitly in Fig. 3, in which the estimated aggregation bias is compared with the
258 "true" aggregation bias for each grid cell at each grid scale. Figures 2 and 3 show that Eq. (15) is generally a
259 good predictor of aggregation bias. Both the estimated aggregation biases (Fig. 2) and the "true" aggregation
260 biases are markedly higher in regions of greater topographic complexity (Fig. S4).

261

262 2.4. Correcting for aggregation bias

263 2.4.1. Identifying drivers of aggregation bias

264 The Taylor expansion in Eq. (15) not only allows one to quantify the aggregation bias; it also allows one to
265 quantify the relative importance of the three input variables (net radiation, soil moisture, and temperature) as
266 drivers of that bias. Each of the terms in Eq. (15) combines a variance or covariance that expresses how
267 variable the input data are, and a second derivative that expresses how sensitive the average ET is to that
268 variability. Each of these terms – a derivative multiplied by a variance or covariance – has the same units as ET,
269 and thus they can be directly compared to one another.

270

271 Table 1 shows each of the aggregation bias terms, calculated over all of Switzerland for the two randomly
272 chosen days mentioned in Sect. 4 (May 31st and July 21st, 2004). For these two example days, the aggregation
273 bias is clearly dominated by a single term, associated with the variance of soil moisture. The variance in net
274 radiation (R_n) creates no aggregation bias, because GLEAM ET is a linear function of R_n ; thus positive and
275 negative deviations from average R_n will increase and decrease ET by exactly offsetting amounts. Similarly, the
276 variance in temperature (T) also results in little aggregation bias, because GLEAM ET increases nearly linearly
277 with T across a wide range of temperature. The covariance terms similarly lead to little aggregation bias. By
278 contrast, the strong curvature in the quadratic dependence of ET on soil moisture (Eq. 6) implies that positive



279 and negative deviations from mean soil moisture will not have offsetting ET effects, and thus that spatial
280 heterogeneity in soil moisture can significantly alter average ET.

281

282 2.4.2. Correcting for aggregation bias using sub-grid closure relationships

283 The Taylor expansion framework in Eq. (7) can be used not only to diagnose aggregation bias, but also to
284 estimate sub-grid closure relationships that correct for the effects of small-scale heterogeneity. The variance
285 and covariance terms in Eq. (7) express how sub-grid heterogeneity affects average ET at the grid scale,
286 implying that these aggregation bias estimates could be used to improve grid-scale ET estimates, without
287 explicitly modeling ET at high resolutions. This approach could be particularly useful in land surface algorithms
288 that are part of coarser-resolution Earth system models; in such cases it may be much more efficient to
289 evaluate Eqs. 7-14 at the coarse grid resolution than to directly evaluate the underlying ET model, Eq. 6, at
290 high resolution. The Taylor expansion approach could also be attractive where we lack spatially explicit high-
291 resolution maps of the ET drivers, but where their variances and covariances can nonetheless be estimated
292 from other sources (such as from the variability of topography, mapped soil units, remote sensing data, etc.).

293

294 It is beyond our scope here to construct such variance and covariance estimates, but we can illustrate how
295 they could potentially be used. The solid red symbols in Fig. 4 show the relationships between "true" average
296 ET and modeled grid-cell-averaged ET, for each grid cell (and one example day, July 21st, 2004) at several
297 different grid scales. For comparison, the open grey symbols in Fig. 4 show average ET estimated by the Taylor
298 expansion approach of Eq. (7), which corrects for sub-grid heterogeneity effects using only grid-cell-averaged
299 estimates of the ET drivers and their small-scale variances and covariances.

300

301 The heterogeneity-corrected ET estimates shown by the open symbols in Fig. 4 cluster much closer to the 1:1
302 line than the modeled grid-cell-averaged ET values shown by the solid red symbols, suggesting that the Taylor
303 expansion approach may substantially improve estimates of grid-cell-averaged ET. Real-world results may be
304 less clear than those shown in Fig. 4, because the heterogeneity-corrected ET estimates (the open symbols in
305 Fig. 4) are calculated using exact values for the variances and covariances of the ET drivers within each grid
306 cell, and in real-world cases these variances and covariances will not be known precisely. Figure 4 nonetheless
307 demonstrates the potential value of knowing, or being able to estimate, those variances and covariances.
308 Efforts to determine those variances and covariances can be focused on the terms that matter the most, if one
309 can identify the main drivers of aggregation bias using the methods described in Sect. 5.1 above.

310

311

312

313

314

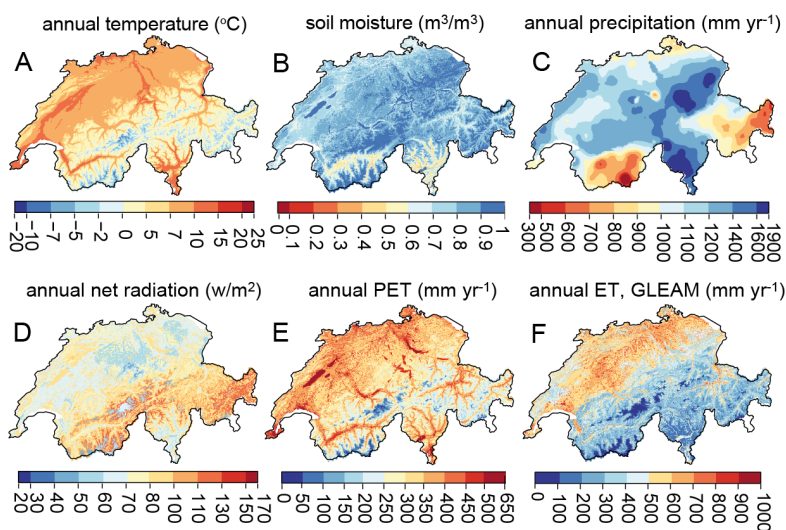


315
 316
 317
 318
 319
 320
 321
 322

Table 1. Relative importance of different ET drivers in aggregation bias estimates (different terms in Eq. 15). Values are calculated for all of Switzerland for the two randomly chosen days (May 31st and July 21st, 2004). The aggregation bias is dominated by the term associated with the variance of soil moisture for these two example days.

	\overline{ET} mm d ⁻¹	\overline{ET} mm d ⁻¹	Bias %	Contribution of $Var(R_n)$ term in % aggregation bias (%)	Contribution of $Var(w_w)$ term in % aggregation bias (%)	Contribution of $Var(T)$ term in % aggregation bias (%)	Contribution of $Cov(R_n, T)$ term in % aggregation bias (%)	Contribution of $Cov(R_n, w_w)$ term in % aggregation bias (%)	Contribution of $Cov(R_n, w_w)$ term in % aggregation bias (%)
Calculation	(Eq. 8)	(Eq. 7)	(Eq. 15)	$\frac{1}{2} \frac{\partial^2 ET}{\partial R_n^2} Var(R_n)$ ($\overline{ET} \cdot Bias$)	$\frac{1}{2} \frac{\partial^2 ET}{\partial w_w^2} Var(w_w)$ ($\overline{ET} \cdot Bias$)	$\frac{1}{2} \frac{\partial^2 ET}{\partial T^2} Var(T)$ ($\overline{ET} \cdot Bias$)	$\frac{\partial^2 ET}{\partial R_n \partial T} Cov(R_n, T)$ ($\overline{ET} \cdot Bias$)	$\frac{\partial^2 ET}{\partial R_n \partial w_w} Cov(R_n, w_w)$ ($\overline{ET} \cdot Bias$)	$\frac{\partial^2 ET}{\partial w_w \partial T} Cov(w_w, T)$ ($\overline{ET} \cdot Bias$)
31.05.2004	2.658	1.636	38.43	0	97.94	0.04	0.48	0.22	1.32
21.07.2004	2.38	1.685	29.16	0	94.67	1.05	3.03	0.33	0.92

323
 324
 325



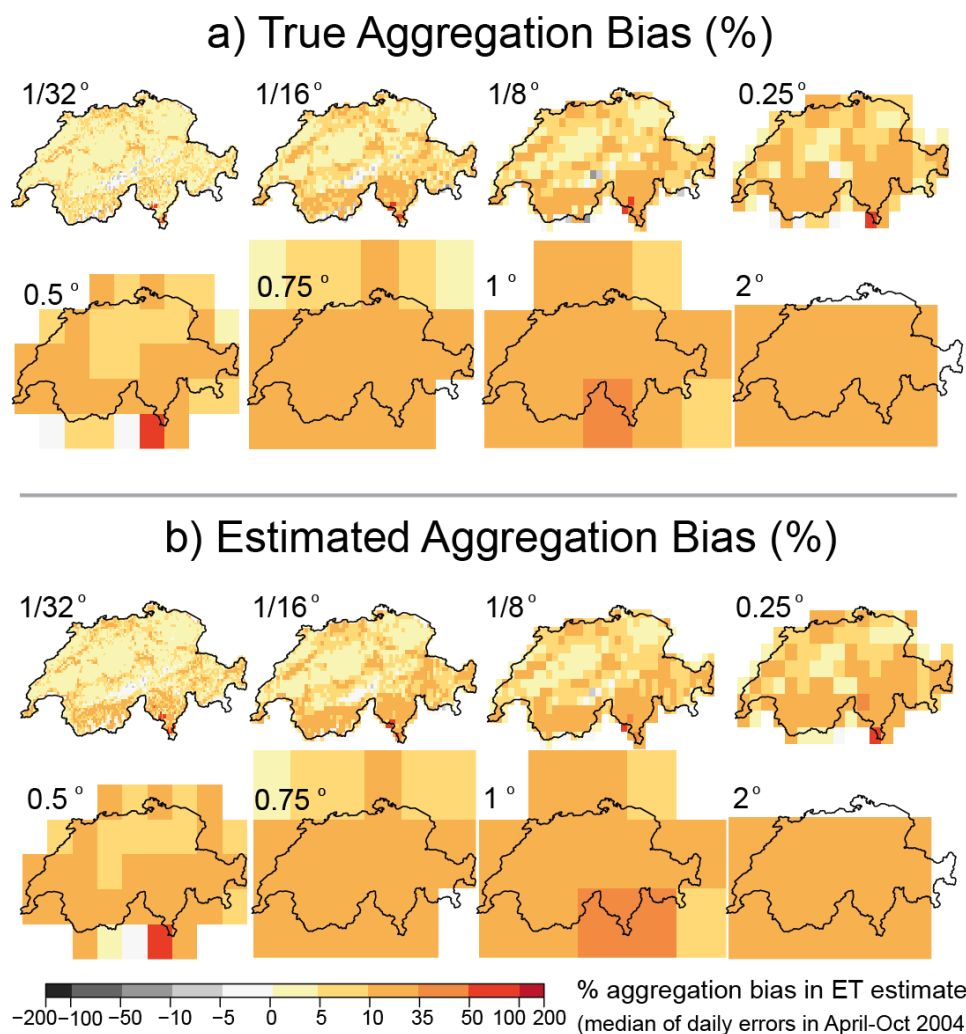
326

Figure 1. Spatial distribution of input data for the year 2004 at 500-m resolution: Annual mean (A) temperature (°C), (B) soil moisture (m³ m⁻³, simulated by the PREVAH hydrological model), (C) precipitation (mm yr⁻¹), (D) net radiation (W m⁻²), (E) potential evapotranspiration (PET, mm yr⁻¹) using the Priestley-Taylor equation (Eq.



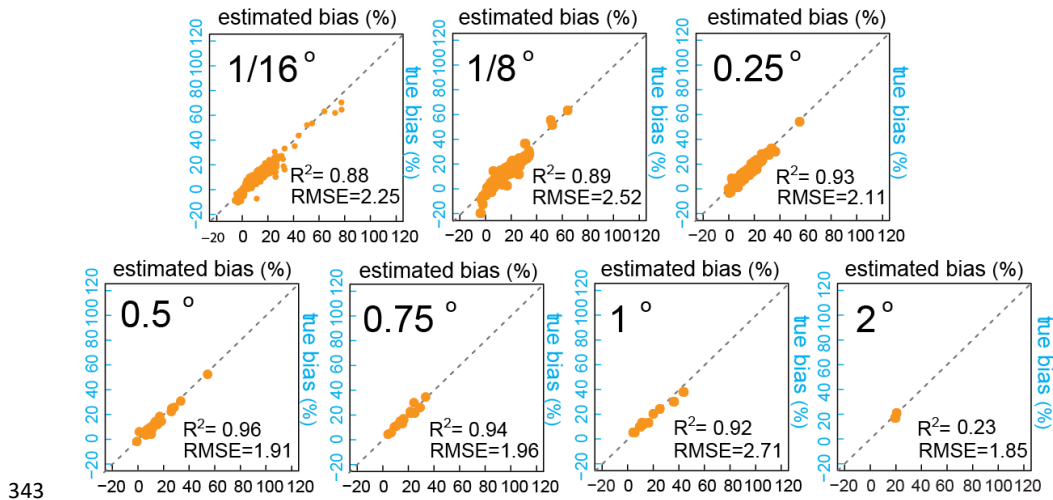
330 3), and (F) evapotranspiration (ET, mm yr⁻¹) using the approach used in the GLEAM model (Eq. 1). See Table. S1
331 for references.

332
333



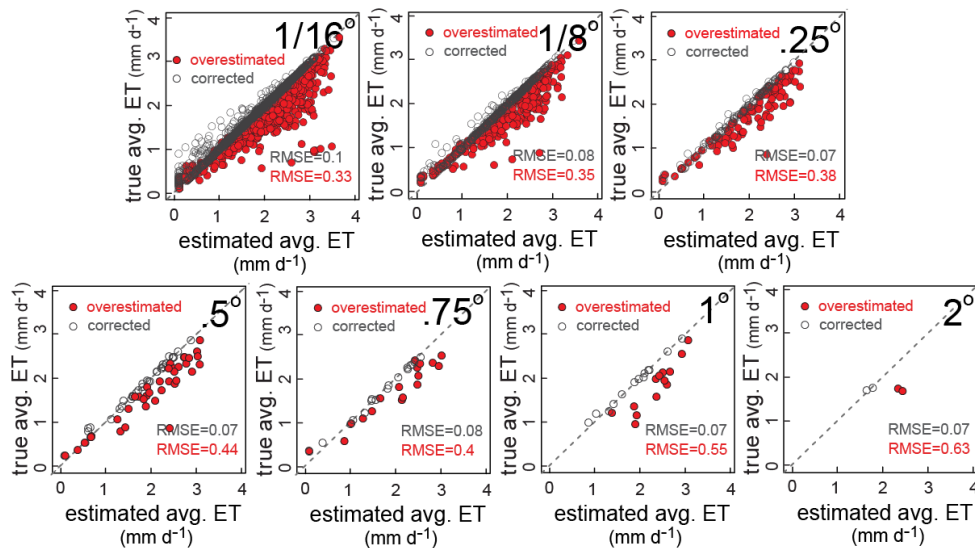
335 Figure 2. a) “True” aggregation bias in ET, as calculated by averaging the 500-m resolution ET estimates using
336 fine-resolution input data in Eq. 6, over 1/32, 1/16, 1/8, 0.25, 0.5, 0.75, 1, and 2-degree grid cells across
337 Switzerland. b) Aggregation bias in ET, as estimated by Eq. 7 from grid-cell averaged temperature (°C), soil
338 moisture (w_w), net radiation (R_n), their variances at each grid scale, and the covariances of all pairs of variables
339 using the 500-m input data. At finer grid scales, the aggregation bias is more localized, and smaller on average.
340 Across Switzerland as a whole, average aggregation bias becomes smaller as grid scales become finer, but
341 never disappears completely.

342



343

344 Figure 3. Daily estimated aggregation bias in ET estimates (% , median of daily biases in Apr.-Oct. 2004) versus
 345 daily true aggregation bias in ET estimates (% , median of daily biases in Apr.-Oct. 2004) at several spatial
 346 scales. Estimated aggregation biases are calculated using Eq. 7. True aggregation biases are calculated as
 347 differences between the finer resolution ET estimates from finer resolution input data, averaged over several
 348 spatial scales (average of functions) and ET values calculated from average inputs at each spatial scale
 349 (function of averages). The coefficients of determination (R^2) between the true and estimated aggregation
 350 biases verify the reliability of the Taylor expansion method and Eq. 7 as estimates of the aggregation bias.



351

352 Figure 4. Daily estimated ET rates versus "true" average ET at each grid cell at several different grid scales
 353 (example day, July 21st, 2004). The solid red symbols demonstrate the relationships between "true" average ET
 354 calculated using fine-resolution data at each grid cell and modeled grid-cell-averaged ET using grid-cell-



355 averaged inputs in Eq.8, for each grid cell at several different grid scales (overestimated). For comparison, the
356 open symbols show true average versus average ET estimated by the Taylor expansion approach of Eq. (7),
357 which corrects for sub-grid heterogeneity effects using only grid-cell-averaged estimates of the ET drivers and
358 their small-scale variances and covariances (heterogeneity-corrected ET estimates, corrected).

359

360 **3. Discussion**

361 Averaging over spatially heterogeneous ET drivers leads to substantial aggregation biases in ET flux estimates
362 from a typical mechanistic large-scale land surface model. This aggregation bias arises from the inherent
363 nonlinearities in evapotranspiration processes, coupled with the inherent spatial heterogeneity in the driving
364 factors. The joint effects of these nonlinearities and heterogeneities can be estimated using second-order
365 Taylor expansions of the governing equations. Using Switzerland as a test case, we have shown that median
366 aggregation biases of 10-35% are common, even at grid scales substantially smaller than those typically used in
367 land surface models (Fig. 2). These biases can be much larger for individual days (Figs. S2 and S3). These biases
368 can have substantial consequences for water and energy flux estimates in land surface models and
369 consequently for temperature predictions in coupled models. The overestimated evaporative fluxes would
370 lead to overestimated latent heat fluxes and underestimated sensible heat fluxes, and thus potentially to
371 underestimates of expected temperature increases in a changing climate. Unrealistically high evaporation
372 estimates lead to cooler modeled temperatures and wetter modeled climates. Correcting for the aggregation
373 bias in ET fluxes would lead to reduced evaporative cooling and increased atmospheric heating via sensible
374 heat flux.

375

376 In coupled Earth system models, ET fluxes influence how surface temperature, net radiation, and soil moisture
377 evolve through time, and thus influence future values of ET. The analyses shown in Figs. 2-4 are based on static
378 values for each day, and thus do not account for the propagation of aggregation biases forward through time.
379 Estimating the consequences of aggregation biases for dynamic modeling would require fully coupled Earth
380 system model simulations rather than the single ET algorithm analyzed here. In a dynamic model, the Taylor
381 expansion approach can potentially be used to correct for aggregation biases in each time step, using
382 statistical models for the variances and covariances of the ET drivers. Thus, estimating aggregation biases in a
383 dynamic model would not require explicitly simulating sub-grid heterogeneity at every time step. Correcting
384 for aggregation biases at each modeling time step would prevent them from propagating further into future
385 time steps, or into the partitioning of future water and energy fluxes at the land surface. The present paper
386 does not illustrate this dynamic correction for aggregation biases, but establishes the theoretical framework
387 for it.

388

389 The purpose of our analysis was to demonstrate how aggregation bias due to spatial heterogeneity can be
390 quantified (Sects. 3-4), how its dominant drivers can be identified (Sect. 5.1), and how its effects can be



391 efficiently corrected for, using sub-grid closure relationships (Sect. 5.2). For this demonstration, we chose
392 GLEAM as an illustrative example, and Switzerland as a topographically complex case study where high-
393 resolution data on the ET drivers are available. Applications of this approach to more complex land surface
394 models may require calculating the necessary derivatives (see Eq. 7) numerically rather than analytically, and
395 applications where high-resolution data are unavailable may require statistically estimating the variances and
396 covariances among the drivers of ET, based on their relationships with topography, soil types, land cover, etc.
397 Using the approach outlined here, one can account for the effects of sub-grid heterogeneity without explicitly
398 modeling ET at fine spatial resolution, which could be impractical due to computational costs, or impossible
399 due to a lack of fine-resolution input data.

400

401 In our analysis, spatial heterogeneity in soil moisture emerged as the dominant driver of aggregation bias in ET
402 estimates. Particularly if this result can also be confirmed in other regions and climates, it points to the
403 importance of improving our understanding of spatial patterns of soil moisture and what controls them. The
404 lower topographic curvature of coarsely gridded landscapes can lead models to predict higher soil moisture at
405 coarser grid scales (Kuo et al., 1999); higher soil moisture at larger grid scales would lead to even higher
406 modeled values of ET, beyond the effects of the aggregation biases analyzed here. Soil moisture may also be
407 substantially influenced by lateral subsurface transfers of water, which are ignored in our analysis and are also
408 ignored by many land surface models. Overlooking lateral transfers could potentially bias ET estimates in large-
409 scale land surface models (Fan et al., 2019), but this is beyond the scope of the present study.

410

411

412 **Acknowledgements**

413 We thank Prof. Ying Fan Reinfelder for numerous insightful discussions and for helpful comments on the
414 manuscript. E.R.F. acknowledges support from the Swiss National Science Foundation (SNSF) under Grant No.
415 P2EZP2_162279.

416 **Data Availability Statement**

417 We will upload the source data for this study to a FAIR repository and provide the URL with the final version of
418 the paper.

419

420



421 **References**

- 422 Beven, K. J., and Cloke, H. L.: Comment on “Hyperresolution global land surface modeling: Meeting a grand
423 challenge for monitoring Earth's terrestrial water” by Eric F. Wood et al., *Water Resour. Res.*, 48, W01801,
424 doi:10.1029/2011WR010982, 2012.
- 425 Beven, K. J.: The holy grail of scientific hydrology: $Q_t=H(SR)A$ as closure, *Hydrol. Earth Syst. Sci.*, 10, 609–618,
426 2006.
- 427 Boone, A., and O. J. Wetzel: A simple scheme for modeling sub-grid soil texture variability for use in an
428 atmospheric climate model. *Journal of the Meteorological Society of Japan*, 77(1), 317–333, 1998.
- 429 Brunner, M. I., Liechti, K., & Zappa, M.: Extremeness of recent drought events in Switzerland: dependence on
430 variable and return period choice. *Natural Hazards and Earth System Science*, 19(10), 2311–2323,
431 <https://doi.org/10.5194/nhess-19-2311-2019>, 2019.
- 432 Brunt, D. *Physical and dynamical meteorology*, 2nd ed., Univ. Press, Cambridge. 428 pp, 1952
- 433 Brutsaert, W., *Evaporation into the atmosphere*, ISBN 978-90-481-8365-4, DOI 10.1007/978-94-017-1497-6,
434 1984.
- 435 BFS, *Die Bodennutzung der Schweiz. Arealstatistik 1979/85*. Bundesamt fuer Statistik, Bern, 1995.
- 436 Budyko, M. I.: *Climate and life*, Academic, New York, 1974.
- 437 Bundesamt für Landestopographie, *Digitales Höhenmodell RIMINI*, Wabern.
438 [https://www.bfs.admin.ch/bfs/de/home/dienstleistungen/geostat/geodaten-](https://www.bfs.admin.ch/bfs/de/home/dienstleistungen/geostat/geodaten-bundesstatistik/topografie.assetdetail.230215.html)
439 [bundesstatistik/topografie.assetdetail.230215.html](https://www.bfs.admin.ch/bfs/de/home/dienstleistungen/geostat/geodaten-bundesstatistik/topografie.assetdetail.230215.html), 1991.
- 440 El Maayar, M. , J. M. Chen: Spatial scaling of evapotranspiration as affected by heterogeneities in vegetation,
441 topography, and soil texture, *Remote Sensing of Environment*, 102, 33–51, 2006.
- 442 Ershadi A., M. F. McCabe, J. P. Evans, J. P. Walker: Effects of spatial aggregation on the multi-scale estimation
443 of evapotranspiration, *Remote Sensing of Environment* 131, 51–62,
444 <http://dx.doi.org/10.1016/j.rse.2012.12.007>, 2013.
- 445 Fan, Y., M. Clark, D. M. Lawrence, S. Swenson, L. E. Band, S. L. Brantley, P. D. Brooks, W. E. Dietrich, A. Flores,
446 G. Grant, J. W. Kirchner, D. S. Mackay, J. J. McDonnell, P. C. D. Milly, P. L. Sullivan, C. Tague, H. Ajami, N.
447 Chaney, A. Hartmann, P. Hazenberg, J. McNamara, J. Pelletier, J. Perket, E. Rouholahnejad-Freund, T. Wagener,
448 X. Zeng, E. Beighley, J. Buzan, M. Huang, B. Livneh, B. P. Mohanty, B. Nijssen, M. Safeeq, C. Shen, W. van
449 Verseveld, J. Volk, D. Yamazaki: Hillslope hydrology in global change research and Earth system modeling,
450 *Water Resources Research*, 55, doi:10.1029/2018WR023903, 2019.
- 451 Gash, J. H. C., an analytical model of rainfall interception by forests. *Q. J. R. Meteorol. Soc.* 105 (433), 43–55,
452 1979.



- 453 Giorgi, F.: An Approach for the Representation of Surface Heterogeneity in Land Surface Models. Part I:
454 Theoretical Framework. *Mon. Wea. Rev.*, 125, 1885–1899, <https://doi.org/10.1175/1520->
455 0493(1997)125<1885:AAFTRO>2.0.CO;2, 1997.
- 456 Giorgi, F., and R. Avissar: Representation of heterogeneity effects in Earth system modeling: Experience from
457 land surface modeling, *Rev. Geophys.*, 35, 413–437, doi:10.1029/97RG01754, 1997.
- 458 Greve, P., B. Orlowsky, B. Mueller, J. Sheffield, M. Reichstein and S. I. Seneviratne: Global assessment of trends
459 in wetting and drying over land, *Nature Geoscience*, 7: 716, 2014.
- 460 Hong, S. H., J. M. H. Hendrickx, and B. Borchers: Up-scaling of SEBAL derived evapotranspiration maps from
461 Landsat (30 m) to MODIS (250 m) scale, *Journal of Hydrology*, 370, 122–138, 2009.
- 462 Huang, X., A. M. Rhoades, P. A. Ullrich, and C. M. Zarzycki, An evaluation of the variable-resolution- CESM for
463 modeling California’s climate, *J. Adv. Model. Earth Syst.*, 8, 345–369, doi:10.1002/2015MS000559, 2016.
- 464 Jasechko, S., Z. D. Sharp, J. J. Gibson, S. J. Birks, Y. Yi and P. J. Fawcett: Terrestrial water fluxes dominated by
465 transpiration, *Nature*, 496: 347, 2013.
- 466 Kuo, W. L., Steenhuis, T. S., McCulloch, C. E., Mohler, C. L., Weinstein, D. A., DeGloria, S. D., and Swaney, D. P.:
467 Effect of grid size on runoff and soil moisture for a variable-source-area hydrology model, *Water Resour. Res.*,
468 35(11), 3419– 3428, doi:10.1029/1999WR900183, 1999.
- 469 Martens, B., D. G. Miralles, H. Lievens, R. van der Schalie, R. A. M. de Jeu, D. Fernández-Prieto, H. E. Beck, W. A.
470 Dorigo and N. E. C. Verhoest, GLEAM v3: satellite-based land evaporation and root-zone soil moisture, *Geosci.*
471 *Model Dev.* 10(5): 1903-1925, 2017.
- 472 McCabe M., and E. Wood: Scale influences on the remote estimation of evapotranspiration using multiple
473 satellite sensors, *Remote Sensing of Environment* 105, 271–285, 2006.
- 474 Miralles, D. G., T. R. H. Holmes, R. A. M. De Jeu, J. H. Gash, A. G. C. A. Meesters and A. J. Dolman: Global land-
475 surface evaporation estimated from satellite-based observations, *Hydrol. Earth Syst. Sci.* 15(2): 453-469, 2011.
- 476 Miralles, D. G., A. J. Teuling, C. C. van Heerwaarden and J. Vilà-Guerau de Arellano: Mega-heatwave
477 temperatures due to combined soil desiccation and atmospheric heat accumulation, *Nature Geosci.* 7(5): 345-
478 349, 2014.
- 479 Miralles, D. G., M. J. van den Berg, J. H. Gash, R. M. Parinussa, R. A. M. de Jeu, H. E. Beck, T. R. H. Holmes, C.
480 Jiménez, N. E. C. Verhoest, W. A. Dorigo, A. J. Teuling and A. Johannes Dolman: El Niño–La Niña cycle and
481 recent trends in continental evaporation, *Nature Climate Change*, 4: 122, 2013.
- 482 Monteith, J.L and M.H. Unsworth, *Principles of Environmental Physics*. Edward Arnold, London, 1990.
- 483 Monteith, J. L.: Evaporation and environment, the state of and movement of water in living organisms,
484 *Proceeding of Soc. for Exp. Biol.*, 19, 205-234, doi:10.1002/qj.49710745102, 1965.



- 485 Mueller, B., M. Hirschi, C. Jimenez, P. Ciais, P. A. Dirmeyer, A. J. Dolman, J. B. Fisher, M. Jung, F. Ludwig, F.
486 Maignan, D. G. Miralles, M. F. McCabe, M. Reichstein, J. Sheffield, K. Wang, E. F. Wood, Y. Zhang and S. I.
487 Seneviratne: Benchmark products for land evapotranspiration: LandFlux-EVAL multi-data set synthesis, *Hydrol.*
488 *Earth Syst. Sci.* 17(10): 3707-3720, 2013.
- 489 Murray, F. W., On the computation of saturation vapor pressure. *J. Appl. Meteor.* 6: 203-204, 1967.
- 490 Orth, R., Staudinger, M., Seneviratne, S. I., Seibert, J., & Zappa, M.: Does model performance improve with
491 complexity? A case study with three hydrological models. *Journal of Hydrology*, 523, 147-159,
492 <https://doi.org/10.1016/j.jhydrol.2015.01.044>, 2015
- 493 Penman, H. L., 'Natural evaporation from open water, bare soil, and grass', *Proc. Roy. Soc. London A*193, 120-
494 146, 1948.
- 495 Priestley, C. H. B., and Taylor, R. J.: On the assessment of surface heat flux and evaporation using large-scale
496 parameters, *Monthly Weather Review*, 100, 81-92, 10.1175/1520-0493(1972)100<0081:otaosh>2.3.co;2,
497 1972.
- 498 Rauscher, S. A., E. Coppola, C. Piani, and F. Giorgi, Resolution effects on regional climate model simulations of
499 seasonal precipitation over Europe, *Clim. Dyn.*, 35(4), 685–711, 2010.
- 500 Ringler, T., L. Ju, and M. Gunzburger, A multiresolution method for climate system modeling: Application of
501 spherical centroidal Voronoi tessellations, *Ocean Dyn.*, 58(5–6), 475–498, 2008.
- 502 Rouholahnejad Freund, E., and J. W. Kirchner: A Budyko framework for estimating how spatial heterogeneity
503 and lateral moisture redistribution affect average evapotranspiration rates as seen from the atmosphere,
504 *Hydrology and Earth System Sciences*, 21(1), 217-233, 2017.
- 505 Rouholahnejad Freund, E., Y. Fan, J. W. Kirchner, Global assessment of how averaging over spatial
506 heterogeneity in precipitation and potential evapotranspiration affects modeled evapotranspiration rates, ,
507 *Hydrol. Earth Syst. Sci. Discuss.*, <https://doi.org/10.5194/hess-2019-103>, in review, 2019.
- 508 Seneviratne, S. I., et al., "Investigating soil moisture–climate interactions in a changing climate: A review",
509 *Earth-Science Reviews* 99(3–4): 125-161, 2010.
- 510 Shrestha, P., M. Sulis, C. Simmer and S. Kollet: Impacts of grid resolution on surface energy fluxes simulated
511 with an integrated surface-groundwater flow model, *Hydrol. Earth Syst. Sci.* 19(10): 4317-4326, 2015.
- 512 Shrestha, P., M. Sulis, C. Simmer and S. Kollet: Effects of horizontal grid resolution on evapotranspiration
513 partitioning using TerrSysMP, *Journal of Hydrology* 557: 910-915, 2018.
- 514 Skamarock, W. C., J. B. Klemp, M. G. Duda, L. D. Fowler, S.-H. Park, and T. D. Ringler, A multiscale
515 nonhydrostatic atmospheric model using centroidal Voronoi tessellations and C-grid staggering, *Mon. Weather*
516 *Rev.*, 140(9), 3090–3105, 2012.



- 517 Speich, M. J. R., Bernhard, L., Teuling, A. J., & Zappa, M.: Application of bivariate mapping for hydrological
518 classification and analysis of temporal change and scale effects in Switzerland. *Journal of Hydrology*, 523, 804-
519 821, <https://doi.org/10.1016/j.jhydrol.2015.01.086>, 2015.
- 520 Stanghellini, C., *Transpiration of Greenhouse Crops*. PhD thesis, Wageningen University, Wageningen, The
521 Netherlands, 1987.
- 522 Tetens, O., *Über einige meteorologische Begriffe*. *z. Geophys.* 6:297-309, 1930.
- 523 Viviroli, D., Zappa, M., Gurtz, J., & Weingartner, R.: An introduction to the hydrological modelling system
524 PREVAH and its pre- and post-processing-tools. *Environmental Modelling and Software*, 24(10), 1209-1222,
525 <https://doi.org/10.1016/j.envsoft.2009.04.001>, 2009.
- 526 Zappa, M. and Gurtz, J.: Simulation of soil moisture and evapotranspiration in a soil profile during the 1999
527 MAP-Riviera Campaign, *Hydrol. Earth Syst. Sci.*, 7, 903–919, <https://doi.org/10.5194/hess-7-903-2003>, 2003.
- 528 Zarzycki, C. M., M. N. Levy, C. Jablonowski, J. R. Overfelt, M. A. Taylor, and P. A. Ullrich, *Aquaplanet*
529 *experiments using CAM's variable-resolution dynamical core*, *J. Clim.*, 27(14), 5481–5503, 2014.
- 530
- 531